ENERGY SCHEME OF THE TELLURIUM VALENCE BAND

M. S. BRESLER, V. G. VESELAGO, Yu. V. KOSICHKIN, G. E. PIKUS, I. I. FARBSHTEĬN, and S. S. SHALYT

Semiconductor Institute and P. N. Lebedev Physics Institute, U.S.S.R. Academy of Sciences

Submitted May 19, 1969

Zh. Eksp. Teor. Fiz. 57, 1479–1494 (November, 1969)

The Shubnikov–de Haas effect is investigated in tellurium single crystals with hole concentration p between 2×10^{16} and 2×10^{18} cm^{-3} in magnetic fields up to 100 kOe, in order to determine the structure of the valence band. To interpret the results, group theoretical methods are used to obtain the dispersion law (3) for the two upper valence bands of tellurium and corrections of the order k^4 due to interactions with neighboring bands. The experimental results agree quantitatively with the dispersion law; corrections must be taken into account for $p > 5 \times 10^{17}$ cm^{-3}. The derived dispersion law describes satisfactorily the results of galvanomagnetic investigations in weak and quantized magnetic fields as well as the results obtained from the investigation of cyclotron resonance and magnetooptics. During the study of the Shubnikov–de Haas effect a number of characteristics were observed which can be interpreted using the concept of magnetic breakdown of the trajectory on the Fermi surface corresponding to the given dispersion law.

INTRODUCTION

FOR the description of energy band structures in semiconductors we must first determine the positions of the energy extremes in k space and the dispersion law $\epsilon(\mathbf{k})$ in the vicinity of these extremal points. The energy spectrum of current carriers in tellurium has been the subject of several investigations by different methods.

An investigation of the galvanomagnetic properties of lightly doped tellurium single crystals having hole concentrations 10^{14}–10^{15} cm^{-3} has indicated that the constant-energy surfaces of the valence band can be represented by ellipsoids of revolution having the principal axis parallel to the C_3 crystal axis.[1] This general conclusion was confirmed in experiments on cyclotron resonance; it was shown that the ellipsoids are elongated along the C_3 axis, i.e., $m_{\parallel} > m_{\perp}$.[2,3]

A theoretical calculation of scattering anisotropy was the basis for harmonizing the conclusions regarding the ellipsoidal shape that followed from galvanomagnetic and cyclotron data.[4] However, these experiments could not be used to determine either the number of ellipsoids or their positions in the Brillouin zone. An analysis of the optical properties of tellurium[5] and some theoretical calculations[6] led Hulin and Picard to conclude that the valence band extrema are located on the lateral edges of a hexagonal prism representing the Brillouin zone of tellurium, and close to the vertices of trihedral angles (the points M and P in Fig. 1).

Based on our experimental investigation[7] of the Shubnikov–de Haas (Sh-dH) quantum oscillations of magnetoresistance in static fields up to 40 kOe in the cases of tellurium single crystals having hole concentrations 4×10^{16}–1×10^{17} cm^{-3}, we have proposed a band model according to which at low energies the Fermi surface consists of four prolate ellipsoids of revolution (with spin taken into account). In[8], where the magnetooptics of tellurium was investigated, Hardy and Rigaux presented, without derivation, Hulin's dispersion law, corresponding to that model, for the valence band. The model accounts for much of the experimental data, include the optical results.[8]

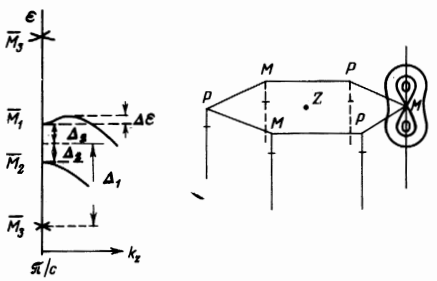

FIG. 1. Energy scheme of tellurium at the point M, and constant energy surfaces in the tellurium Brillouin zone (shown schematically). At P the terms $\bar{M}_1$ and $\bar{M}_2$ are interchanged. Energy is measured from a level halfway between the $\bar{M}_1$ and $\bar{M}_2$ bands.

The complicated shape of the energy surface was discovered through our experimental investigation of Sh-dH quantum oscillations in tellurium single crystals with $p \approx 1 \times 10^{17}$ cm^{-3}.[7] Braun and Landwehr[9] investigated samples with concentrations 10^{17}–6×10^{18} cm^{-3} in pulsed fields up to 220 kOe. From a detailed study of a sample with the concentration 1.5×10^{18} cm^{-3} they concluded that the Fermi surface is barrel-shaped with circular symmetry about the C_3 axis. Guthman and Thuillier[10] investigated tellurium single crystals with 1.2×10^{17}–6×10^{18} holes/cm^3 in pulsed magnetic fields. They concluded, in qualitative agreement with the calculations of Hulin and Picard, that the Fermi surface has a dumbbell shape for high densities.

In a brief communication[11] we have presented preliminary experimental results showing how the periods of Sh-dH oscillations vary with the current carrier concentration. It was shown that if in the region of concentrations 2×10^{16}–1×10^{17} cm^{-3} the Fermi surface can be represented by an ellipsoid of revolution, then for 10^{17}–10^{18} cm^{-3} it becomes a more complex dumbbell-shaped surface of revolution with its center at the

point M; this results from the junction of two closely-lying "bulging" ellipsoids.[1)]

Further refinement of the hole energy scheme of tellurium was made possible by an improved technique for measuring the Sh-dH effect in heavily doped crystals. To begin with, it was necessary to go from pulsed fields to a high static magnetic field. This was achieved using the "Solenoid" apparatus described in[13], which permitted static fields up to 100 kOe. Some of the preliminary results that we obtained with this apparatus have been reported in[14].

The conditions for the observation of Sh-dH quantum oscillations of the magnetoresistance ($\epsilon_F \gg kT$, $\hbar\Omega \gg kT$, $\Omega\tau \gg 1$) are fulfilled in tellurium with hole concentrations $p \gtrsim 10^{17}$ cm^{-3} at helium temperatures in magnetic fields $H > 20$ kOe; here ϵ_F is the Fermi energy, Ω is the cyclotron frequency, and τ is the relaxation time of the carriers.

We know that for an arbitrary closed Fermi surface the period of the Sh-dH oscillations in a quasiclassical approximation is determined by the extremal intersection of the surface S_φ with a plane perpendicular to the magnitude field:

$$\Delta\left(\frac{1}{H}\right)=\frac{2\pi e}{\hbar c}\frac{1}{S_\varphi}. \qquad (1)$$

(Here φ is the angle between the direction of the magnetic field H and the C_3 axis.)

When a few extremal sections exist the experimentally observed pattern consists of superimposed oscillations having different periods that are determined by these cross sections. By varying the angle φ we determine a set of extremal cross sections of the Fermi surface in different directions and thus determine the shape of the latter.[15] However, experience has shown that when investigating the Fermi surfaces of metals it is more efficient to discuss the experimental results on the basis of the theoretical model and to determine the parameters of this model from experiment.

As already mentioned, group-theoretical considerations lead to an analytic form of the dispersion law for the energy bands in tellurium, and thus to the construction of the model.

THEORY

The valence band of tellurium at the point M has three branches corresponding to the representations $\overline{M}_1$, $\overline{M}_2$, and $\overline{M}_3$, resulting from the spin-orbit splitting of the doubly degenerate (neglecting spin) representation M_3. Since only relatively small splitting of these branches occurs, to determine the spectrum at fairly high energies we must take all three branches into account. To construct the matrix $\mathcal{H}(\mathbf{k}, \mathbf{H})$ for the representation M_3, whereby we determine the spectrum in a magnetic field for all three branches, we have used the method of invariants.[16]

The representation M_3 pertains to the case b_3, since the points $\mathbf{k}_0$ and $-\mathbf{k}_0$ are included in different "stars." Therefore, according to Eq. (8) of[16], $\mathcal{H}(\mathbf{k}, \mathbf{H})$ in this case includes functions of k, H, and σ that we transformed according to the representations $M_3 \times M_3 = \Gamma_1 + \Gamma_2 + \Gamma_3$. These functions are given in Table I. Included here are functions of σ describing the spin-orbit interaction, nonrelativistic terms that are linear and quadratic in k, and σk terms determining the relativistic corrections to the spectrum that are linear in k. All these components have been chosen to permit identical transformations; this is a necessary condition for the method of invariants.

The basis matrices, transforming according to the representations Γ_1, Γ_2, and Γ_3, are taken in the form

$$I,\ \rho_3=\begin{vmatrix}1 & 0\\ 0 & -1\end{vmatrix},\quad \rho_+=\begin{vmatrix}0 & 1\\ 0 & 0\end{vmatrix},\quad \rho_-=\begin{vmatrix}0 & 0\\ 1 & 0\end{vmatrix} \qquad (1a)$$

and we shall assume that they transform like I, J_z, J_+, and J_-, respectively. It was shown in[16] that these matrices can be chosen arbitrarily to a certain extent. Then $\mathcal{H}(\mathbf{k}, \mathbf{H})$ will be given by

$$\begin{aligned}\hat{\mathcal{H}} = {} & I\{\lambda+\alpha_1\sigma_z k_z+\alpha_2(\sigma_+k_-+\sigma_-k_+)\\ & +\gamma_1\sigma_z H_z+\gamma_2(\sigma_+H_-+\sigma_-H_+)\}\\ & +\rho_3\{\Delta_1\sigma_z+B_1k_z+i\alpha_3(\sigma_+k_--\sigma_-k_+)\\ & +g_1H_z+i\gamma_3(\sigma_+H_--\sigma_-H_+)\}\\ & +\rho_+\{\Delta_2\sigma_-+B_2k_-+A_3k_+^2+iA_4k_-k_z+\alpha_4\sigma_+k_++i\alpha_5\sigma_-k_z\\ & +i\alpha_6\sigma_zk_-+g_2H_-+\gamma_4\sigma_+H_++i\gamma_5\sigma_-H_z+i\gamma_6\sigma_zH_-\}\\ & +\rho_-\{\Delta_2\sigma_++B_2k_++A_3k_-^2-iA_4k_+k_z+\alpha_4\sigma_-k_--i\alpha_5\sigma_+k_z\\ & -i\alpha_6\sigma_zk_++g_2H_+-\gamma_4\sigma_-H_--i\gamma_5\sigma_+H_z-i\gamma_6\sigma_zH_+\}; \qquad (2)\end{aligned}$$

where $\lambda = A_1k_z^2 + A_2k_\perp^2$.

We have included in $\mathcal{H}$ relativistic and nonrelativistic terms that are linear in H, in order to elucidate the character of the spin splitting. Although the $\overline{M}_1$ and $\overline{M}_2$ bands are nondegenerate, the extrema at the points $\mathbf{k}_0$ and $-\mathbf{k}$ can in principle be shifted in opposite directions in a magnetic field. In the present case, as will be seen below [specifically in (4) and (5a)], band splitting does not occur in the approximation that is linear in H, but is proportional to $H_+^3 + H_-^3$. The operator $\mathcal{H}$ can be written at once for holes, i.e., the minimum hole energy corresponds to the upper valence band $\overline{M}_1(\overline{M}_2)$. All constants in (2) are real; the constants α_i and γ_i are relativistically small. Replacing the σ_i operators with Pauli matrices, we can write the matrix $\mathcal{H}(\mathbf{k}, \mathbf{H})$ at once.

Table I. Distribution of functions of k, σ, and H among the irreducible representations

Γ_1	I	—	—	$k_z^2,\ k_\perp^2$	$\sigma_+k_-+\sigma_-k_+,\ \sigma_zk_z$	—	$\sigma_+H_-+\sigma_-H_+,\ \sigma_zH_z$
Γ_2	ρ_3	σ_z	k_z	—	$\sigma_+k_--\sigma_-k_+$	H_z	$\sigma_+H_--\sigma_-H_+$
Γ_3	$\rho_+,\ \rho_-$	$\sigma_+,\ \sigma_-$	$k_+,\ k_-$	$k_-^2,\ k_+^2,$ $k_+k_z,\ -k_-k_z$	$\sigma_-k_-,\ \sigma_+k_+,\ \sigma_zk_+,$ $-\sigma_zk_-,\ \sigma_+k_z,\ -\sigma_-k_z$	$H_+,\ H_-$	$\sigma_-H_-,\ \sigma_+H_+,\ \sigma_zH_+,$ $-\sigma_zH_-,\ \sigma_+H_z,\ -\sigma_-H_z$

If the energy $\epsilon(\mathbf{k})$ is much smaller than the splitting of the bands $\overline{M}_1$, $\overline{M}_2$, and $\overline{M}_3$ bands, we finally obtain $\epsilon(\mathbf{k})$ in a form coinciding with that given by Hulin:[8]

$$\varepsilon(k) = A_1k_z^2+A_2k_\perp^2 \pm [\Delta_2^2+((B_1-\alpha_1)^2+\alpha_5^2)k_z^2]^{1/2}. \qquad (3)$$

[1)]The formation of a dumbell-shaped energy surface at sufficiently high energies is also confirmed by the most recent measurements of cyclotron resonance in tellurium.[13] We are indebted to Dr. P. L. Radoff and Professor R. Dexter for detailed information about their work.

Table II

No. of sample	p, 10^{17} cm^{-3} ($T = 1{,}8°$ K)	u, $\frac{\text{cm}^2}{\text{V-sec}}$ ($T = 1.8°$ K)	$S_\perp$, 10^{13} cm^{-2} ($H \perp C_3$)	$S_\parallel$, 10^{13} cm^{-2} ($H \parallel C_3$)		$\Delta S_\parallel$, 10^{13} cm^{-2}
				S_m	S_0	
1	2.12	4480	1.45/0.657	4.77	2.51	2.26
2	2.47	4070	1.45/0.672	5.15	2.89	2.26
3	3.04	4770	1.80	6.15	4.33	1.82
4	3.30	4280	1.86	6.50	3.98	2.52
5	5.00	3560	2.48	8.90	6.03	2 87
6	7.15	4400	2.82	11.5	8.08	3.42
7	15.7	3730	4.77	22.5	17.2	5.30
8	21.4	3140	6.10	31.8	23.8	8.00

We observe that when relativistic terms linear in k are taken into account the form of the spectrum is not affected. The dispersion law (3) corresponds to the band scheme in tellurium near M_1 that is shown in Fig. 1. The spectrum of $\epsilon(k)$ at k = 0 in a magnetic field is given by

$$\varepsilon = \pm(\Delta_2^2 + \gamma_5^2 H_z^2)^{1/2}, \tag{4}$$

and thus, as already mentioned, contains no terms that are linear in H.

At high energies the contribution from band splitting must be taken into account. If we here retain nonrelativistic terms up to k^4 and relativistic terms up to k^2, inclusively, we obtain

$$\varepsilon = A_1 k_z^2 + \left(A_2 - \frac{B_3^2}{2\Delta_1}\right)k_\perp^2 - \frac{1}{2\Delta_1}\{A_3^2 k_\perp^4 + A_4^2 k_\perp^2 k_z^2 + B_2 A_3 (k_+^3 + k_-^3) - iA_3 A_4 k_z (k_+^3 - k_-^3)\} \pm \left[\left(\Delta - \frac{\beta^2 k_\perp^2}{2\Delta_1}\right)^2 + ((B_1 - \alpha_1)^2 + \alpha_5^2) k_z^2\right]^{1/2}, \tag{5}$$

where[2)]

[2)] $\beta^2 = \alpha_2'^* B_2' + \alpha_2' B_2'^*$, $B_3^2 = B_2^2 + \alpha_2^2 + \alpha_3^2 + \alpha_6^2$, $B_2' = B_2 - i\alpha_6$, $\alpha_2' = \alpha_2 - i\alpha_3$.

EXPERIMENTAL RESULTS

Preliminary investigations of samples with hole concentration $p \sim 3 \times 10^{17}$ cm^{-3}, as well as data given by other investigators,[9,10] have indicated cylindrical symmetry of the Fermi surface about the C_3 axis.

In the present work we present results obtained with tellurium samples grown by the Czochralski method along the C_3 crystallographic direction with hole concentrations from 10^{17} to 2×10^{18} cm^{-3} at 4.2°K. Antimony was used as the dopant. The orientation of the crystal axes was verified by means of cleavage planes. A chromium polishing etchant was applied to the surfaces of the samples.[11] The properties of the samples are given in Table II.

The apparatus permitted rotation of the samples about a horizontal axis. In this way we varied the angle between the magnetic field direction and the C_3 axis of the crystal in a plane perpendicular to the length of the sample. The samples were in direct contact with liquid helium. The results to be discussed were obtained at 1.8°K.

[2)] The expression for $\epsilon(H)$ at the point $\mathbf{k}_0$ (k = 0) with the inclusion of H^3 terms is similar:

$$\varepsilon(H) = \gamma'(H_+^3 + H_-^3) \pm [\Delta_2 + \gamma''(H_+^3 + H_-^3)]. \tag{5a}$$

At $-\mathbf{k}_0$, H is replaced by −H. Terms proportional to H^2, which result in an identical shift at the points $\mathbf{k}_0$ and $-\mathbf{k}_0$, are here omitted.

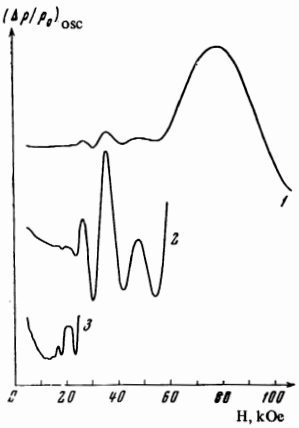

FIG. 2

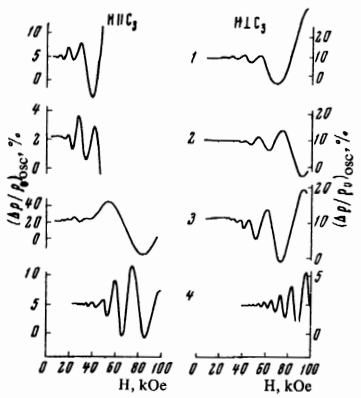

FIG. 3

FIG. 2. Shubnikov – de Haas effect for sample No. 6 with $\mathbf{H} \parallel C_3$. Curves 2 and 3 are the initial segments of curve 1 enlarged 10 and 50 times, respectively.

FIG. 3. A comparison of the quantum oscillations of magnetoresistance in tellurium samples with different hole concentrations for the two principal orientations of the magnetic field with respect to the C_3 axis. 1 – p = 2.12 × 10^{17} cm^{-3}, 2 – p = 3.04 × 10^{17} cm^{-3}, 3 – p = 5 × 10^{17} cm^{-3}, 4 – p = 2.14 × 10^{13} cm^{-3}.

The Hall effect was measured by averaging results obtained for two sample orientations that differed by 180°. All the experimental curves were traced using the two-coordinate automatic recording device described in[7]. The apparatus enabled us to register reliably the oscillations of magnetoresistance in low magnetic fields when the oscillations were only one-tenth as high as those in the maximum fields (Fig. 2).

Figure 3 shows the results obtained from our investigation of Sh-dH oscillations in tellurium single crystals having different hole concentrations, for the two principal orientations of the magnetic field with respect to the trigonal axis. We observe that for $\mathbf{H} \perp C_3$ the curves exhibit the exponential increase of oscillatory amplitude that is ordinarily found in the Sh-dH effect. For $\mathbf{H} \parallel C_3$ the clearly observed beats indicate the existence of more than one extremal cross section of the Fermi surface for this direction of the magnetic field. In accordance with (1), when a single extremal cross section exists the maxima of the oscillations are equally spaced on the inverse magnetic field scale. Figures 4 and 5 show the experimentally observed positions of the maxima for samples Nos. 1 and 5 at different angles φ. For sample No. 5 equal spacing occurs only in the range $60° \lesssim \varphi \lesssim 90°$, whereas for No. 1 such spacing is absent at all angles. Also, in both cases the angular dependence

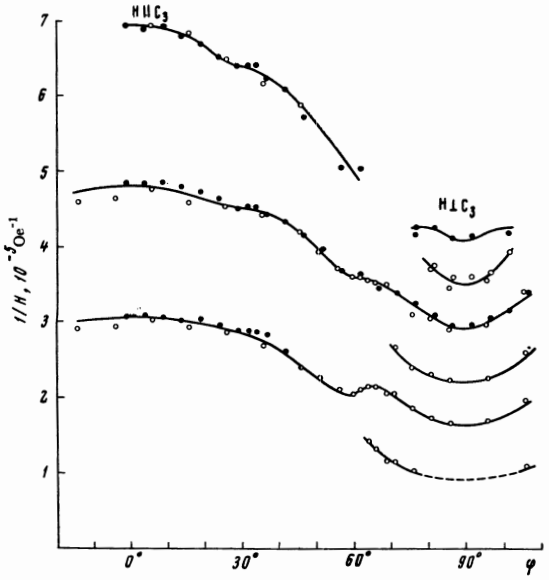

FIG. 4. Angular dependence [$\varphi = \sphericalangle(C_3, H)$] of the positions of magnetoresistance maxima on the 1/H scale for sample No. 1 ($p = 2.12 \times 10^{17}$ cm^{-3}). The dots represent measurements up to 40 kOe in an SP-47 magnet; the open circles represent measurements up to 100 kOe in the "Solenoid."

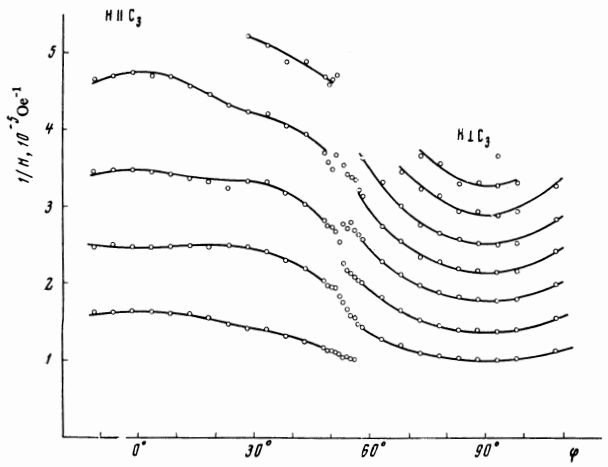

FIG. 5. Angular dependence of the positions of magnetoresistance maxima on the 1/H scale for sample No. 5 ($p = 5 \times 10^{17}$ cm^{-3}).

of the positions of the maxima reveals a singularity near $\varphi = 60°$.

The beats observed on the oscillation curves, manifested by nonmonotonic dependence of the oscillation amplitude on the ordinal number of the maximum and by the absence of oscillatory periodicity with respect to the inverse field, indicate that more than one extremal cross section of the Fermi surface exists. Since the energy surface model corresponding to the dispersion law (3) predicts two different extremal cross sections for magnetic field directions parallel to or close to the trigonal axis, we developed the following method of analyzing the experimental curves.

When two cross sections exist the oscillatory portion of the magnetoresistance can be represented on the 1/H scale as the superposition of two exponentially damped harmonics:

$$\Delta\rho_{osc} \sim a_1 \exp\left(-\frac{\delta_1}{H}\right) \sin\left(\frac{c\hbar}{eH} S_1 + \beta_1\right) + a_2 \exp\left(-\frac{\delta_2}{H}\right) \sin\left(\frac{c\hbar}{eH} S_2 + \beta_2\right). \quad (6)$$

We therefore used a simulating scheme consisting of two oscillatory contours with adjustable decrements and intrinsic frequencies. The contours were excited by identical pulses from two G5-15 generators, which were used with internal delay lines for creating the necessary phase shift between the oscillations of the contours. The signals were combined by the differential amplifier of an S1-17 oscillograph. The resultant curve was projected from the oscillograph screen, thus producing a graph that represented the oscillatory portion of the experimental $\rho(H)$ curve on the 1/H scale. By adjusting the contour parameters and the phase shift we matched the experimental and simulating curves. The experimentally observed oscillations could thus be resolved into components corresponding to the two extremal cross sections of the Fermi surface, thus determining the parameters S_i, β_i, and δ_i in (6).

Figure 6 illustrates the resolution into components. The phase difference $\beta_1 - \beta_2$ between the two components was in most cases close to $\pi/2$. This was consistent with a quasiclassical treatment that considered the phase difference of oscillations corresponding to the minimum and maximum cross sections.[17] The described analysis of the experimental data enabled us to measure the extremal cross sections of the Fermi surface for samples with different concentrations and at different angles $\varphi = \sphericalangle(H, C_3)$. Values for the principal extremal cross sections ($H \parallel C_3$ and $H \perp C_3$) are given in Table II.

In addition to the discussed oscillations of magnetoresistance we observed oscillations, small in absolute magnitude (at most 3%), of the Hall coefficients R_1 and R_3, which were shifted by about one-half period relative to the magnetoresistance oscillations ($\Delta\rho/\rho_0$).

DISCUSSION OF RESULTS

The experimental results were interpreted using a

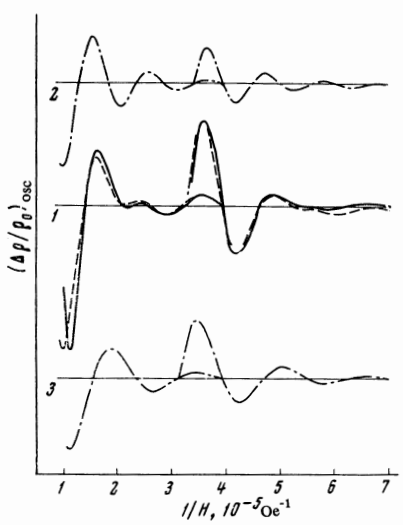

FIG. 6. Resolution of the experimental beat pattern into components corresponding to two extremal cross sections of the Fermi surface: 1 – A comparison of the (solid) experimental curve with the (dashed) simulating curve; 2 and 3 – separated components. The curves on the right side of the graph have been amplified 10 times as compared with the curves on the left side.

Fermi surface model corresponding to the dispersion law (3). The parameters of the energy scheme are determined as follows.

Near the valence band maximum [the point $(\pm k_z^m, 0)$] the energy surface is represented by two ellipsoids of revolution about the C_3 axis. Therefore two combinations of the constants in (3) can be determined from the longitudinal and transverse effective masses that are derived by investigating cyclotron resonance in samples with $p \sim 10^{14}$ cm^{-3} at helium temperatures. We obtain

$$\frac{1}{m_{\parallel}} = \frac{2A_1}{\hbar^2}\left(1 - \frac{4A_1^2\Delta_2^2}{C^4}\right), \quad \frac{1}{m_{\perp}} = \frac{2A_2}{\hbar^2}, \tag{7}$$

where $C^2 \equiv (B_1 - \alpha_1)^2 + \alpha_5^2$. From[2] we obtain $m_{\parallel} = 0.24\ m_0$, $m_{\perp} = 0.126\ m_0$, and from[3] we obtain $m_{\parallel} = 0.264\ m_0$, $m_{\perp} = 0.109\ m_0$. In calculating the dispersion law parameters we used the mean values

$$m_{\parallel} = 0.252\ m_0, \quad m_{\perp} = 0.117\ m_0, \tag{7a}$$

which lead to the mass anisotropy $m_{\parallel}/m_{\perp} = 2.2$; this agrees with the result obtained in[7] from the Sh-dH effect in samples with $p < 10^{17}$ cm^{-3}.

Two other constants in the dispersion law can be determined from optical measurements. Indeed, $2\Delta_2$ is the energy of the direct optical transition between the valence bands $\bar{M}_1$ and $\bar{M}_2$ (Fig. 1). Optical investigations can also be used to determine the energy difference between the point $(k_z^m, 0)$ corresponding to the maximum energy in the $\bar{M}_1$ band and the point (0, 0) (a saddle point):

$$\Delta\varepsilon = -\frac{\Delta_2^2 A_1}{C^2} - \frac{C^2}{4A_1} + \Delta_2. \tag{8}$$

Hardy and Rigaux[8] observed two optical transitions (at 126.3 and 128.6 MeV) between the valence bands of tellurium. These can be interpreted as transitions between the $\bar{M}_1$ and $\bar{M}_2$ bands with the transition energies $2\Delta_2$ and $2\Delta_2 + \Delta\epsilon$, so that $\Delta\epsilon = 2.3$ MeV.[3)] This interpretation of the 128.6-MeV transition can be disputed, although the dispersion law (3) does provide another possible way of determining $\Delta\epsilon$. We note that the difference $S_m - S_0$ between the areas of the extremal cross sections for $\mathbf{H} \parallel C_3$ is given by

$$S_m - S_0 = \frac{\pi}{A}\Delta\varepsilon \tag{9}$$

and is independent of the Fermi energy. This fact can be used to test the fulfillment of the dispersion law (3).

The described method of determining the energy parameters from experimentally measured quantities yields the following values:

$$\begin{aligned} A_1 &= 0.363 \cdot 10^{-14}\ \text{eV-cm}^2 \\ A_2 &= 0.326 \cdot 10^{-14}\ \text{eV-cm}^2 \\ C^2 &= 0.06 \cdot 10^{-14}(\text{eV})^2\text{-cm}^2 \end{aligned} \tag{10}$$

In the quasiclassical approximation the experimentally determined periods of Sh-dH oscillations enable us to calculate the extremal cross sections of the Fermi surface for different Fermi energies (i.e., for different concentrations) and for different orientations of the magnetic field relative to the trigonal axis of a crystal. To compare theory with experiment we must calculate the theoretical extremal cross sections of the Fermi surface that follow from the assumption of the dispersion law (3). The carrier concentration assuming complete degeneracy is determined by the volume of k space that is enclosed inside the Fermi surface corresponding to a given energy. An electronic computer was used to calculate, on the basis of (3) and (10), the energy dependences of the volume and extremal cross sections of the Fermi surface. We also plotted energy contours in the $k_z k_\perp$ plane, which are shown in Fig. 7 for different levels of valence band occupation.

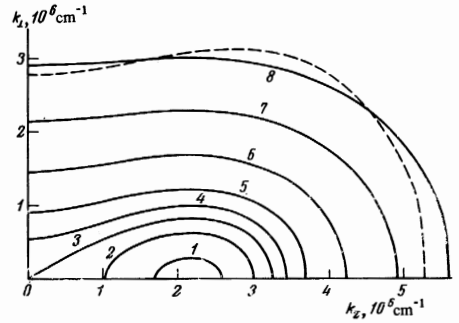

FIG. 7. Constant-energy contours in the $k_z k_\perp$ plane, corresponding to the dispersion relation (3) for different hole concentrations (p): 1 – 2.75×10^{15} cm^{-3}, 2 – 2.60×10^{16} cm^{-3}, 3 – 6.47×10^{16} cm^{-3}, 4 – 1.19×10^{17} cm^{-3}, 5 – 2.12×10^{17} cm^{-3}, 6 – 4.94×10^{17} cm^{-3}, 7 – 1.08×10^{18} cm^{-3}, 8 – 2.14×10^{18} cm^{-3}. The dashed curve was calculated from (5), which includes correction terms up to k^4, for $p = 2.14 \times 10^{-3}$.

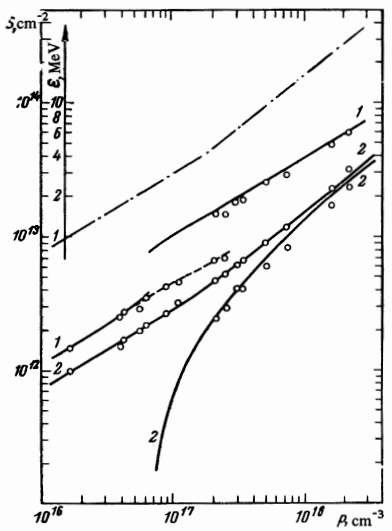

FIG. 8. Calculated and experimental dependences of the principal extremal cross sections of the Fermi surface on hole concentration, for: 1 – $\mathbf{H} \perp C_3$, 2 – $\mathbf{H} \parallel C_3$. Solid curves – calculated; open circles – experimental; dot-dash curve-concentration dependence of the Fermi surface. Energy is calculated from the top of the $\bar{M}_1$ valence band.

Figure 8 compares the concentration dependences of the calculated and experimental extremal cross sections of the Fermi surface. The given data were obtained in[7,11] for $p \lesssim 10^{17}$ cm^{-3}.

Figure 9 shows the calculated and experimental

[3)] It is of interest that in [18], where stimulated recombination emission from tellurium was investigated in the energy region corresponding to interband transitions, two lines also separated by 2.3 MeV were observed.

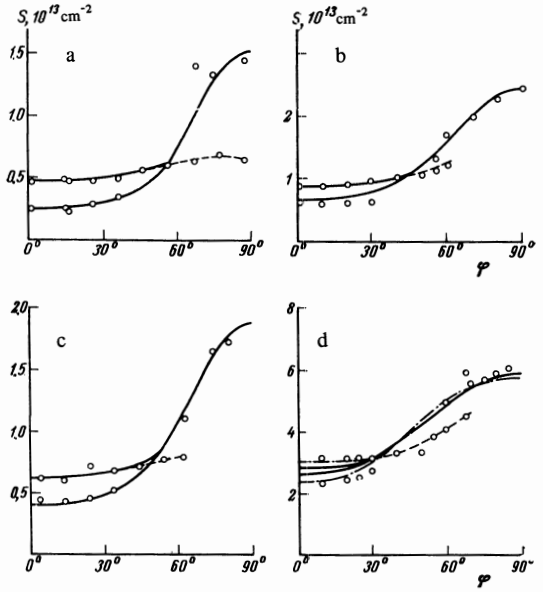

FIG. 9. Experimental and calculated angular dependences of the Fermi-surface extremal cross sections for tellurium samples with different hole concentrations. a – sample No. 1 ($p = 2.12 \times 10^{17}$ cm^{-3}), b – No. 3 ($p = 3.04 \times 10^{17}$ cm^{-3}), c – No. 5 ($p = 5 \times 10^{17}$ cm^{-3}), d – No. 8 ($p = 2.14 \times 10^{18}$ cm^{-3}). Solid curves – calculated from (3); open circles – experimental; dot-dash curve – calculated from (5).

angular dependences of the extremal cross sections for samples with different hole concentrations. In some cases for samples with $p \leq 5 \times 10^{17}$ cm^{-3} the Fermi energy for the best agreement between experiment and the calculations corresponded to a concentration that differed only slightly (by at most 5%) from the concentration based on the Hall effect. This difference lies within the limits of accuracy for determining the Hall coefficient.

The presented data demonstrate the good agreement between the experimental results for concentrations $p \leq 5 \times 10^{17}$ cm^{-3} and calculations based on the dispersion law (3). We therefore conclude that this law represents, for the given concentration region, all the experimental data derived from investigations of the galvanomagnetic, optical, and resonance effects.

For samples with $p > 5 \times 10^{17}$ cm^{-3} the experimental values differ appreciably from the calculations (see Fig. 8 and Fig. 9c, d). This discrepancy cannot be eliminated by obtaining more precise carrier concentrations. It can be assumed that the disagreement is associated with the approximate character of the dispersion law (3). Figure 10 shows the concentration dependence of $\Delta\epsilon$ determined from the difference $S_m - S_0$. For low p we observe that $\Delta\epsilon$ is actually independent of the concentration and is close to the value 2.3 MeV that we have taken on the basis of optical data. However when $p > 5 \times 10^{17}$ cm^{-3}, $\Delta\epsilon$ begins to increase with the concentration (i.e., with increase of the Fermi energy); this indicates that the energy spectrum here begins to deviate from (3).

At high energies the approximation that takes into account only the interaction of the two uppermost valence bands can be inadequate. In this case the angular and concentration dependences of the extremal cross sections must be described by the dispersion law (5),

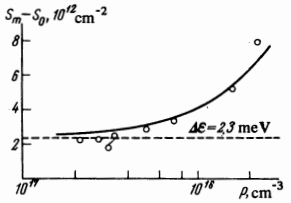

FIG. 10. Difference between the extremal cross sections of the Fermi surface for H || C_3 versus hole concentration. Dashed line – based on Eq. (3); solid curve – based on Eq. (5).

which takes into account the perturbation-theoretical terms in k^3 and k^4 that result from interactions of the $\overline{M}_1$ and $\overline{M}_2$ bands with bands having $\overline{M}_3$ symmetry (the lowest valence band and the conduction band). It follows from (5) that the inclusion of $\overline{M}_3$ bands leads to a renormalized coefficient of the term that is proportional to $k_\perp^2$, although this is not essential for a comparison between theory and experiment. In the comparison with the experimental results we neglected the relativistically small term $\beta^2 k_\perp^2 / 2\Delta_1$. In calculating the extremal cross sections we also neglected terms containing $k_\perp^3 \cos 3\Phi$ and $k_z k_\perp^3 \sin 3\Phi$ that destroy cylindrical symmetry, because it is evident that in first approximation for H || C_3 these terms do not affect the cross-sectional area of the Fermi surface; Φ is the azimuthal angle.

A calculation based on (5) with the foregoing assumptions yielded the angular dependence shown by the dot-dash curve in Fig. 9d. The Fermi surface is then distorted (shown by the dashed curve in Fig. 7). This effect may have led Braun and Landwehr to the conclusion that tellurium has a barrel-shaped Fermi surface.[9]

By means of curve fitting we found the following values of the constants $A_3^2/2\Delta_1$ and $A_4^2/2\Delta_1$ that best fit the experimental data:

$$\frac{A_3^2}{2\Delta_1} = 0.6 \cdot 10^{-28} \text{ eV-cm}^4 \quad \frac{A_4^2}{2\Delta_1} = 0.4 \cdot 10^{-28} \text{ eV-cm}^4 \qquad (11)$$

When we calculate Δ_1, taking the ratio $\Delta_1/\Delta_2 = 1.9$ from the numerical calculations of Picard and Hulin,[6] we obtain the following values of the constants A_3 and A_4 in units of $\hbar^2/2m_0$:

$$A_3 = 9.8, \quad A_4 = 8.0, \qquad (11a)$$

and, in the same units,

$$A_1 = 9.5, \quad A_2 = m_0 / m_\perp = 8.55. \qquad (11b)$$

The concentration dependence of the difference $S_m - S_0$ between the extremal cross sections, calculated from (5) and (11), is shown by the solid curve in Fig. 10.

The spread of the experimental results prevents us from assuming that we have obtained reliable values of the parameters in (11). Furthermore, for high concentrations the experimental values of the principal cross sections were sensitive to disturbances of the correct orientation between the crystal axes and the axis of the sample. It is evident that to describe the experimental results in a broad range of concentrations (up to 2×10^{18} cm^{-3}) we require a more accurate form of the dispersion law (5).

In Fig. 8 for $p \sim 10^{17}$ cm^{-3} and in Fig. 9 for $\varphi > 50°$ we also find experimentally observed extremal cross sections whose existence does not follow from the quasiclassical investigation that we have described. As we

have mentioned in[14], these cross sections may have resulted from magnetic breakdown of electron orbits that are close to a self-intersecting trajectory.

MAGNETIC BREAKDOWN

According to the dispersion law (3) the family of energy surfaces shown in Fig. 7 includes a surface (curve 3) corresponding to the calculated concentration $p_{cr} = 6.5 \times 10^{16}$ cm^{-3}, such that a carrier moving on this surface in a field $H \perp C_3$ will describe a self-intersecting trajectory. It has been shown in[19,20] that this motion cannot be investigated in the quasiclassical approximation. A quantum-mechanical analysis shows that in this case two trajectories can be realized simultaneously—a completely dumbbell-shaped trajectory and another that is ellipsoidal with one-half the area. Since it is meaningful to consider the position of a carrier accurately down to l^{-1} on a specific trajectory in k-space [$l = (c\hbar/eH)^{1/2}$ is the magnetic length], carriers can tunnel quantum-mechanically from one orbit to another when the separation of two ellipsoidal orbits for concentrations $p < p_{cr}$, or the neck of a dumbbell-shaped trajectory for $p > p_{cr}$, is commensurable with l^{-1}. Electron tunneling from one quasiclassical orbit to another has been called magnetic breakdown.[21] In an exact solution this qualitative picture of carrier behavior in a magnetic field corresponds to the splitting of levels associated with the small (ellipsoidal) cross section of the Fermi surface into two subsystems.

An exact criterion for the simultaneous appearance of two orbits in magnetic breakdown for a symmetric trajectory with a constriction is[20]

$$|\varkappa| = \frac{|\varepsilon - \varepsilon_0|}{2e\hbar H} c \sqrt{m_1 m_2} \lesssim \frac{1}{3}, \qquad (12)$$

where ϵ is the carrier energy, ϵ_0 is the energy represented by a self-intersecting surface, $m_1 = \hbar^2/2A_2$, $m_2 = \hbar^2[2(C^2/2\Delta_2 - A_1)]^{-1}$. The calculations show that for sample No. 1 ($p = 2.1 \times 10^{17}$ cm^{-3}) magnetic breakdown of the central cross section can be observed in fields $H \gtrsim 50$ kOe. Indeed, for this sample with $H \perp C_3$ two cross sections are observed, whereas for this field orientation only one extremal cross section should be observed quasiclassically. In sufficiently high fields magnetic breakdown should also be observed for samples with hole concentrations below the critical value p_{cr}. For example, with $p = 4 \times 10^{16}$ cm^{-3} Eq. (12) gives $H \gtrsim 20$ kOe. This range of concentrations in fields up to 100 kOe is being investigated at the present time.

For samples with $p > 3 \times 10^{17}$ cm^{-3} breakdown of the central cross section of the Fermi surface does not occur with $H \perp C_3$, although we could possibly observe additional oscillations associated with breakdown of nonextremal "oblique" cross sections. Azbel' has shown[20] that in addition to the oscillations corresponding to extremal cross sections of the Fermi surface we can observe oscillation peaks that are associated with nonextremal trajectories close to a self-intersecting trajectory. Oscillations of this kind are observable in Fig. 9.

In this case, however, the results of[20] cannot be applied directly, because the calculation of trajectories for the corresponding values of the angle φ did not reveal self-intersecting orbits. All the calculated trajectories are greatly elongated and have a narrow region with a width of the order of l^{-1} (i.e., they have a long "tongue"). An exact analysis of the experimental results pertaining to magnetic breakdown in tellurium could be based only on numerical calculations of the energy scheme in a magnetic field. In the quasiclassical approximation and the first quantum correction thereof we must confine ourselves to only the foregoing qualitative discussion.[4)]

As a band subject to the dispersion law (3) is filled the probability of magnetic breakdown falls off sharply in association with the approach to ellipsoidal trajectories. However, according to dispersion law (5), the relative deformation of the Fermi surface begins to become enhanced again for high concentrations (the dashed curve in Fig. 7). In this case, for $H \perp C_3$ or orientations close thereto we find oscillations that are associated with noncentral self-intersecting trajectories. The experimentally observed reduction of the range of φ where magnetic breakdown is observed as the concentration increases from 2×10^{17} to 5×10^{17} cm^{-3} (Fig. 9, a—c), and the new large region of φ where an "extra" period is observed for sample No. 8 (Fig. 9d), agree qualitatively with our analysis.

For a Fermi surface with a neck Azbel'[23] predicts an anomalous growth of the oscillatory amplitude in a narrow angular range, because $\partial s/\partial \epsilon$ vanishes for a self-intersecting cross section that is tangent to the neck. (Here S is not the total cross sectional area, but is the area lying at only one end of the neck.) This could possibly account for our observation in[7] of an anomalous increase (by a factor of 7!) in the oscillatory amplitude near $\varphi \approx 60°$ for a sample with $p \sim 10^{17}$ cm^{-3} (Fig. 7 in[7]).

We believe that magnetic breakdown represents the most reasonable explanation of the experimental singularities of Sh-dH oscillations that we have described here and that are not amenable to a simple quasiclassical analysis. It should be noted, however, that additional oscillatory periods in the considered model of the energy scheme could result from a nonuniform distribution of carriers in a sample. Qualitative considerations show, however, that in this case the observed smaller cross section will at most correspond to p_{cr}, i.e., it should not grow with the concentration; this result conflicts with experiment.

The authors are indebted to Academician A. M. Prokhorov for his interest and support; to V. B. Anzin, L. S. Dubinskaya, and D. V. Mashovets for experimental assistance and analysis; to M. B. Klugerman for assistance with the preparation of samples; and to A. G. Aronov and Yu. M. Gal'perin for discussions of the results.

[1] R. V. Parfen'ev, A. M. Pogarskiĭ, I. I. Farbshteĭn,

[4)] Ruvalds and McClure [22] have calculated the energy scheme numerically in a magnetic field for a band model like that of tellurium. Unfortunately they considered only the high-energy case with carriers filling both bands ($\overline{M}_1$ and $\overline{M}_2$ in our terminology), and only for $H \perp C_3$. Their calculation predicts magnetic breakdown here, and for the only low-energy case that they consider is consistent with our present analysis.

and S. S. Shalyt, Fiz. Tverd. Tela 4, 3596 (1962) [Sov. Phys.-Solid State 4, 2630 (1962)].
[2] J. H. Mendum and R. N. Dexter, Bull. Am. Phys. Soc. 9, 632 (1964).
[3] J. C. Picard and D. L. Carter, J. Phys. Soc. Japan 21, Suppl., 202 (1966).
[4] L. S. Dubinskaya and I. I. Farbshteĭn, ZhETF Pis. Red. 2, 307 (1965) [JETP Lett. 2, 195 (1965)].
[5] M. Hulin, J. Phys. Chem. Solids 27, 441 (1966).
[6] M. Picard and M. Hulin, Phys. Stat. Solidi 23, 563 (1967).
[7] L. S. Dubinskaya, G. E. Pikus, I. I. Farbshteĭn, and S. S. Shalyt, Zh. Eksp. Teor. Fiz. 54, 754 (1968) [Sov. Phys.-JETP 27, 402 (1968)].
[8] D. Hardy and C. Rigaux, Solid State Commun. 5, 889 (1967).
[9] E. Braun and G. Landwehr, J. Phys. Soc. Japan 21, Suppl., 380 (1966).
[10] C. Guthman and J. M. Thuillier, Proc. Intern. Symposium on Se and Te, Montreal, 1967; Solid State Commun. 6, 835 (1968).
[11] L. S. Dubinskaya, V. A. Noskin, I. G. Tatiev, I. I. Farbshteĭn, and S. S. Shalyt, ZhETF Pis. Red. 8, 79 (1968) [JETP Lett. 8, 47 (1968)].
[12] P. L. Radoff and R. N. Dexter, Bull. Am. Phys. Soc. 14, 330 (1969).
[13] V. G. Veselago, L. P. Maksimov, and A. M. Prokhorov, Pribory i tekhnika éksperimentov No. 4, 192 (1968).
[14] M. S. Bresler, I. I. Farbstein, D. V. Mashovets, Yu. V. Kosichkin, and V. G. Veselago, Phys. Lett. 29A, 23 (1969).
[15] I. M. Lifshitz and A. V. Pogorelov, Dokl. Akad. Nauk SSSR 96, 1143 (1954).
[16] G. E. Pikus, Zh. Eksp. Teor. Fiz. 41, 1258 and 1507 (1961) [Sov. Phys.-JETP 14, 898 and 1075 (1962)].
[17] I. M. Lifshitz and A. M. Kosevich, Zh. Eksp. Teor. Fiz. 29, 730 (1955) [Sov. Phys.-JETP 2, 636 (1956)].
[18] C. B. Benoit à la Guillaume and J. M. Debever, Solid State Commun. 3, 19 (1965).
[19] G. E. Zil'berman, Zh. Eksp. Teor. Fiz. 34, 748 (1958) [Sov. Phys.-JETP 7, 513 (1958)].
[20] M. Ya. Azbel', Zh. Eksp. Teor. Fiz. 39, 878 and 1276 (1960) [Sov. Phys.-JETP 12, 608 and 891 (1961)].
[21] I. M. Lifshitz and M. I. Kaganov, Usp. Fiz. Nauk 78, 411 (1962) [Sov. Phys.-Uspekhi 5, 878 (1963)].
[22] J. Ruvalds and J. W. McClure, J. Phys. Chem. Solids 28, 509 (1967).
[23] M. Ya. Azbel', Zh. Eksp. Teor. Fiz. 45, 2022 (1963) [Sov. Phys.-JETP 18, 1388 (1964)].

Translated by I. Emin
173